Substantia
An International Journal of the History of Chemistry

Firenze University Press
www.fupress.com/substantia

Research Article

Synthesis, Structural Characterization, and Biological Evaluation of (*E*)-*N*-(4-Bromobenzylidene)-3-Methoxybenzohydrazide Monohydrate

Kumar Ananthi[1], Haridhass Anandalakshmi[1,*], Amaladoss Nepolraj[2], Saravanan Akshaya[1]

[1] *Department of Chemistry, Annamalai University, Annamalai Nagar, 608 002, Tamil Nadu, India*
[2] *Department of Chemistry, PGP College of Arts and Science, Paramathi, Namakkal, 637 207, Tamil Nadu, India*
E-mail addresses: anathikumar13@gmail.com; anandalakshmi74@yahoo.com; nepolraj@gmail.com; akshayasaravanan21@gmail.com
*Corresponding author.

Abstract. Synthesis and structural elucidation of a new type of hydrazone Schiff base *(E)-N'*-(4-Bromobenzylidene)-3-Methoxybenzohydrazide Monohydrate, and its structure were characterized by FT-IR, ^{1}H, ^{13}C NMR and mass spectroscopic analysis. The single crystals of (4-BRMBH) were grown from the DMSO solvent, orthorhombic system with $P2_12_12_1$ space group through single-crystal X-ray diffraction analysis. DFT calculations were performed to understand the electronic properties including frontier molecular orbitals (FMO), molecular electrostatic potentials, and global chemical reactivity descriptors. Intermolecular interactions in the crystal structures were obtained using the Hirshfeld surface analysis. The majority contribution to the Hirshfeld surface is H···H (39.5%) contacts. The molecular docking study were carried out by *in silico* method to analyse their anti-tuberculosis aspect against InhA, the enoyl acyl carrier protein reductase from *Mycobacterium tuberculosis*. Finally, chemical absorption, distribution, metabolism, excretion, and toxicity (ADMET) properties were determined.

Keywords: hybrid crystals, π···π interactions, molecular docking, Hirshfeld surface, ADMET.

OPEN ACCESS

Citation: Ananthi, K., Anandalakshmi, H., Nepolraj, A., & Akshaya, S. (2024) Synthesis, Structural Characterization, and Biological Evaluation of (*E*)-*N*-(4-Bromobenzylidene)-3-Methoxybenzohydrazide Monohydrate. *Substantia* 8(1): 25-38. doi: 10.36253/Substantia-2294

Received: Aug 28, 2023

Revised: Dec 18, 2023

Just Accepted Online: Dec 29, 2023

Published: Mar 04, 2024

Data Availability Statement: All relevant data are within the paper and its Supporting Information files.

Competing Interests: The Author(s) declare(s) no conflict of interest.

INTRODUCTION

The compounds having azomethine functional group –C=N– are recognized as Schiff bases [1]. Schiff bases are a class of mixes that can be effortlessly set up from the buildup of essential amines or amino alcohols with carbonyl mixes [2,3]. The presence of various substituents on both the amine and carbonyl-containing moieties could change their underlying and electronic properties of the compound. A little change in either moiety may

affect in a sizeable modification of their structural and functional behavior [1,4]. Such properties have energized researchers of various fields, for example, precious stone specialists, material researchers, organic chemists, and so forth to center their considerations on Schiff bases [5–17]. The Schiff base hydrazone core has additionally pulled in much consideration in the fields of drug and restorative science [18, 19] due to hydrazide subsidiary was recently announced as a powerful and specific inhibitor for antibacterial-antifungal [20], calming [21], antimalarial [22], *Entamoebahistolyica* [23], against tuberculosis exercises [24]. For every one of these reasons underlying conduct of the Schiff bases has been accounted.

In the present study, we report the synthesis of compound $C_{15}H_{15}BrN_2O_3$ derived from benzohydrazide *via* Schiff base route, bromophenyl ring attached to benzo hydrazidee complex has effective inhibitory activity against various antibacterial activities. Benzohydrazide heterocycles are very good bio isosteres of esters and aldehydes, which has a pharmacological activity by hydrogen-bonding interactions with receptors. In view with the above importance of compound, we have done the structural confirmation by single crystal X-ray crystallography. Since, X-ray diffraction has become indispensable tool in crystal chemistry as it helps in solving the molecular structure, magnitudes and directional characteristics. In view of these, in the present work the XRD analysis of title compound is reported to understand its molecular interactions, conformation and packing modes along with studying configuration. Single crystal studies for the synthesized compound and the results are depicted here. The compounds were characterized by IR, ^{1}H, ^{13}C and mass spectroscopy. DFT studies have been employed to explain the electronic properties of molecules as a dipolarophile. We report the spectral, structural and biological properties of the compounds. Molecular docking and the Hirshfeld surface analysis with d_{norm} and 2D fingerprint plots were performed and their results are discussed.

2. RESULTS AND DISCUSSION

2.1. Spectral data

The IR spectrum of the compound is showed that the IR (KBr, cm^{-1}): (C=O amide, 1652), (NH, 3206), (CH aliphatic, 2837–3079), (C=N, 1580), (C–H aromatic, 3079). The ^{1}H and ^{13}C NMR spectra are the amide proton signal at 11.8 ppm, CH=N– signal at 8.4 ppm singlet (azomethine proton), the proton couplings between 7.81 and 7.16 ppm indicate the presence of aromatic protons in

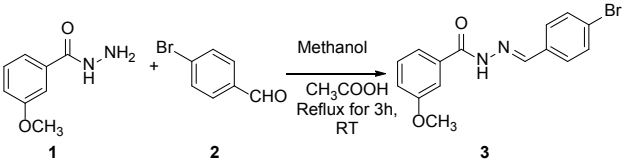

Scheme 1. General produce of (E)-N¢-(4-bromobenzylidene)-3-methoxybenzohydrazide.

^{1}H NMR spectrum. The OCH_3 proton was indicated by a singlet at 3.84 ppm. In ^{13}C NMR spectrum is carbonyl (NH–C=O) signal was observed at 163 ppm, aromatic and CH=N– signals at 120–150 ppm, methoxy carbon signal at 55.8 ppm. The crystal structure supports the mass spectral data as well as the m/z = 333.10 [M$^+$].

2.2. Single crystal XRD

The crystals of single crystal X-ray diffraction analysis revealed that the title compoundwas crystallized in the Orthorhombic crystal system, with $P2_12_12_1$ space group. The unit cell parameters for the compound are a = 4.7974(3) Å, b = 12.5672(9) Å, c = 25.3675(16) Å, b = 90.77° and Z = 4, 1529.40(17) Å^3, and the symmetry code of the molecule in the crystal unit is (i) x–1/2, –y+1/2; (ii) x+1/2, –y+1/2, z–1/2; (iii) x+1, y, z–1; (iv) x–1, y, z+1. The bond parameter such as bond length (Å), bond angle (°), dihedral angle (°) and hydrogen interactions are shown in Tables 2, 3 and 4 were measured. In this water also involved in the hydrogen bonding interaction, but it does not change symmetry, there was observed a negligible influence due to the water present. The structure parameters were calculated and compared with X-ray diffraction bond parameters, for example, the carbonyl (C=O) bond length was observed as about 1.229 Å, were as the calculated value was about 1.228 Å. Similarly, the observed C=N (1.262 Å), C–N (1.337 Å), C–O (1.375 Å), and C–C in ring (1.44–1.35 Å) bond lengths are matches well with the computed parameters. The hydrogen bonding (HB) interactions have been observed like D–H, H···A, D···A and D–H···A among the closest molecule, the donor nitrogen makes the intermolecular hydrogen bonding with the closest neighboring oxygen (O3) atom in the hydroxybenzylidene, its D···A hydrogen bonding distance is about 0.85 Å, similarly O(3)–H(3B)···O(1)#1, O(3)–H(3A)···O(1)#2 (Table 4) shows the intermolecular hydrogen bonding value 0.84 and 0.83.

The determined structure was optimized by density functional theory (DFT) calculation (Fig. 1). The ORTEP diagram of 4-BRMBH with displacement ellipsoids drawn at 50% probability level is shown in Fig. 2. The

Table 1. Crystal data and structure refinement for 4-BRMBH crystal.

Identification code	4-BRMBH
Empirical formula	$C_{15}H_{15}BrN_2O_3$
Formula weight	351.20
Temperature (K)	296(2)
Wavelength (Å)	0.71073
Crystal system	Orthorhombic
Space group	$P2_12_12_1$
Unit cell dimensions	a = 4.7974(3) Å a = 90°
	b = 12.5672(9) Å b = 90°
	c = 25.3675(16) Å g = 90°
Volume (Å^3)	1529.40(17)
Z	4
Density (calculated) (g cm^{-3})	1.525
Absorption coefficient (mm^{-1})	2.699
F(000)	712
Crystal size (mm^3)	0.150 ´ 0.100 ´ 0.100
q Range for data collection (°)	2.281 to 25.019
Index ranges	–4 £h £5, –14 £k £14, –30 £l £29
Reflections collected	19553
Independent reflections	2690 [R(int) = 0.0505]
Completeness to q =25.019°	99.7%
Absorption correction	Semi-empirical from equivalents
Max. and min. transmission	0.7451 and 0.5892
Refinement method	Full-matrix least-squares on F^2
Data/restraints/parameters	2690/4/201
Goodness-of-fit on F^2	1.006
Final R indices [I> 2s(I)]	R_1 = 0.0403, wR_2 = 0.0895
R indices (all data)	R_1 = 0.0822, wR_2 = 0.1070
Absolute structure parameter	0.004(7)
Extinction coefficient	n/a
Largest diff. peak and hole (e Å^{-3})	0.520 and –0.587
CCDC	1839157

details of the crystal data and structure refinement are given in Table 1. The title compound exists in the amido form with a C8–O1 bond length of 1.228(7) Å. The molecule has an E conformation with respect to the azomethine bond, which is confirmed by the torsion angle C4–C7–N1 of 179.1(6)°. The two aromatic rings (C1–C6 and C9–C13), are almost planar hydrazone moiety. There is an intramolecular O–HN, O–H, C–H hydrogen bonding present in the molecule as N2–H(2A)–O3, O3–H(3A)–O1,O3–H(3B)–O1, C7–H7–O3. In this compound both intermolecular and intramolecular hydrogen bonding were occurs shown in Fig. 3a.

This compound is an example of a system where a single atom acts both as donor and acceptor. There are also C–HO (water) contacts present enclosing ring motifs (Fig. 3b). Finally, sheets are formed lying parallel.

Figure 1. Optimized molecular structure of 4-BRMBH crystal.

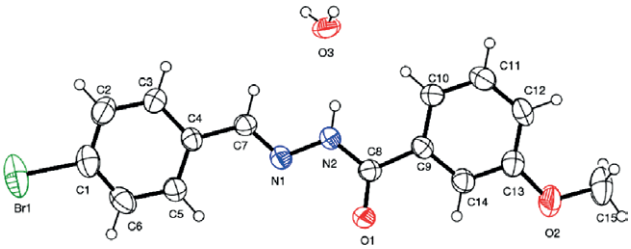

Figure 2. ORTEP of 4-BRMBH crystal.

There are weak-interactions within the sheets involving the bromine-bearing aromatic ring of the molecule. A supramolecular network is built in the lattice by means of intermolecular N–H···O and two O···H–O interactions together with non-classical C–H···O interactions involving the lattice water molecule stacking the molecules along the b-axis direction shown in Fig. 3c.

The resulted bond lengths and bond angles are in good agreement with the standard values, and the list of all the bond lengths, bond angles and torsional angles are presented in Tables. 2 and 3. Both intermolecular and intramolecular hydrogen bonding details for compound 4-BRMBH listed in Table 4.

2.3. Hirshfeld surface analysis

Three-dimensional (3D) molecular Hirshfeld surfaces and the two-dimensional (2D) fingerprint plots represent a new way of visualizing and analyzing intermolecular interactions in molecular crystals. The molecular Hirshfeld surface [33] of a crystal is created by dividing space in the crystal into regions where the electron distribution of sum of atoms for the molecule dominates the corresponding sum over the crystal. Hirshfeld surfaces and their related fingerprint plots are generated using the program Crystal Explorer 3.0 [34]. The crystallographic information file (cif) is given as input to the Crystal Explorer program. The Hirshfeld surface

Table 2. Bond lengths (Å) and bond angles (°) for 4-BRMBH crystal.

Bond lengths (Å)					
C(1)–C(6)	1.354(10)	C(7)–N(1)	1.262(7)	C(12)–H(12)	0.9300
C(1)–C(2)	1.371(10)	C(7)–H(7)	0.9300	C(13)–C(14)	1.374(9)
C(1)–Br(1)	1.898(7)	C(8)–O(1)	1.228(7)	C(13)–O(2)	1.375(8)
C(2)–C(3)	1.363(9)	C(8)–N(2)	1.334(8)	C(14)–H(14)	0.9300
C(2)–H(2)	0.9300	C(8)–C(9)	1.494(8)	C(15)–O(2)	1.398(9)
C(3)–C(4)	1.384(8)	C(9)–C(14)	1.378(8)	C(15)–H(15A)	0.9600
C(3)–H(3)	0.9300	C(9)–C(10)	1.380(8)	C(15)–H(15B)	0.9600
C(4)–C(5)	1.378(8)	C(10)–C(11)	1.373(10)	C(15)–H(15C)	0.9600
C(4)–C(7)	1.448(8)	C(10)–H(10)	0.9300	N(1)–N(2)	1.379(7)
C(5)–C(6)	1.387(9)	C(11)–C(12)	1.365(10)	N(2)–H(2A)	0.85(3)
C(5)–H(5)	0.9300	C(11)–H(11)	0.9300	O(3)–H(3A)	0.83(2)
C(6)–H(6)	0.9300	C(12)–C(13)	1.370(9)	O(3)–H(3B)	0.84(2)
Bond angles (°)					
C(6)–C(1)–C(2)	121.4(6)	N(1)–C(7)–C(4)	122.5(6)	C(12)–C(13)–C(14)	119.8(6)
C(6)–C(1)–Br(1)	120.0(6)	N(1)–C(7)–H(7)	118.7	C(12)–C(13)–O(2)	124.7(6)
C(2)–C(1)–Br(1)	118.6(6)	C(4)–C(7)–H(7)	118.7	C(14)–C(13)–O(2)	115.5(6)
C(3)–C(2)–C(1)	118.3(7)	O(1)–C(8)–N(2)	122.1(6)	C(13)–C(14)–C(9)	121.2(6)
C(3)–C(2)–H(2)	120.8	O(1)–C(8)–C(9)	120.9(6)	C(13)–C(14)–H(14)	119.4
C(1)–C(2)–H(2)	120.8	N(2)–C(8)–C(9)	117.1(5)	C(9)–C(14)–H(14)	119.4
C(2)–C(3)–C(4)	122.2(6)	C(14)–C(9)–C(10)	118.7(6)	O(2)–C(15)–H(15A)	109.5
C(2)–C(3)–H(3)	118.9	C(14)–C(9)–C(8)	116.7(5)	O(2)–C(15)–H(15B)	109.5
C(4)–C(3)–H(3)	118.9	C(10)–C(9)–C(8)	124.6(6)	H(15A)–C(15)–H(15B)	109.5
C(5)–C(4)–C(3)	118.1(6)	C(11)–C(10)–C(9)	119.4(6)	O(2)–C(15)–H(15C)	109.5
C(5)–C(4)–C(7)	123.2(6)	C(11)–C(10)–H(10)	120.3	H(15A)–C(15)–H(15C)	109.5
C(3)–C(4)–C(7)	118.6(6)	C(9)–C(10)–H(10)	120.3	H(15B)–C(15)–H(15C)	109.5
C(4)–C(5)–C(6)	119.9(6)	C(12)–C(11)–C(10)	121.7(7)	C(7)–N(1)–N(2)	116.0(5)
C(4)–C(5)–H(5)	120.0	C(12)–C(11)–H(11)	119.2	C(8)–N(2)–N(1)	119.3(5)
C(6)–C(5)–H(5)	120.0	C(10)–C(11)–H(11)	119.2	C(8)–N(2)–H(2A)	120(5)
C(1)–C(6)–C(5)	120.0(6)	C(11)–C(12)–C(13)	119.1(6)	N(1)–N(2)–H(2A)	120(5)
C(1)–C(6)–H(6)	120.0	C(11)–C(12)–H(12)	120.4	C(13)–O(2)–C(15)	119.2(6)
C(5)–C(6)–H(6)	120.0	C(13)–C(12)–H(12)	120.4	H(3A)–O(3)–H(3B)	113(4)

was obtained using the CIF file data from single crystal XRD analysis. The contact distances d_{norm} is based on d_e express the distances of the nearest nucleus external and d_i is the internal to the surface respectively. The shape index in the molecule structure indicates the shape of the electron density, surface around the molecular interactions. In Fig. 3 (a–d), the deep in red circular indicates hydrogen bonding contacts, whereas the bright red areas in the surface plot indicate H···O and O···H dominant interactions. The light color range area represents longer and weaker contacts [35].

The intercontact in the crystal packing of the title compound 4-BRMBH are quantized using Hirshfeld surface computational analyses. The red-colored spots over the Hirshfeld surface indicate the intercontacts involved in the intermolecular interactions [33,34]

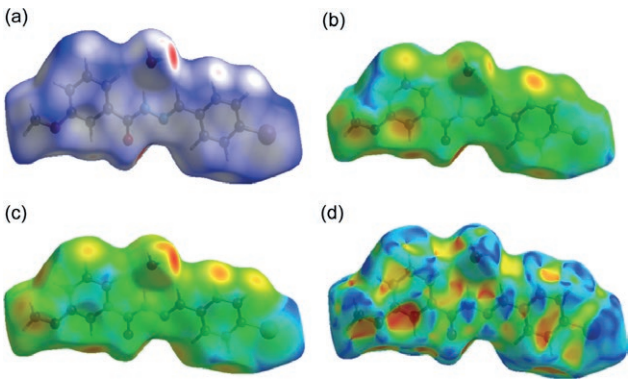

Figure 3. Hirshfeld surfaces of 4-BRMBH crystal: a) d_{norm}, b) d_e, c) d_i and d) shape index.

Table 3. Torsional angles (°) for 4-BRMBH crystal.

C(6)–C(1)–C(2)–C(3)	–1.4(11)	C(14)–C(9)–C(10)–C(11)	0.1(10)
Br(1)–C(1)–C(2)–C(3)	177.6(5)	C(8)–C(9)–C(10)–C(11)	179.2(6)
C(1)–C(2)–C(3)–C(4)	0.2(10)	C(9)–C(10)–C(11)–C(12)	2.0(11)
C(2)–C(3)–C(4)–C(5)	0.8(10)	C(10)–C(11)–C(12)–C(13)	–2.5(12)
C(2)–C(3)–C(4)–C(7)	–178.6(6)	C(11)–C(12)–C(13)–C(14)	0.9(11)
C(3)–C(4)–C(5)–C(6)	–0.6(10)	C(11)–C(12)–C(13)–O(2)	–179.2(7)
C(7)–C(4)–C(5)–C(6)	178.7(6)	C(12)–C(13)–C(14)–C(9)	1.2(10)
C(2)–C(1)–C(6)–C(5)	1.6(11)	O(2)–C(13)–C(14)–C(9)	–178.7(6)
Br(1)–C(1)–C(6)–C(5)	–177.5(5)	C(10)–C(9)–C(14)–C(13)	–1.7(10)
C(4)–C(5)–C(6)–C(1)	–0.5(11)	C(8)–C(9)–C(14)–C(13)	179.1(6)
C(5)–C(4)–C(7)–N(1)	–0.2(9)	C(4)–C(7)–N(1)–N(2)	–179.6(5)
C(3)–C(4)–C(7)–N(1)	179.1(6)	O(1)–C(8)–N(2)–N(1)	0.1(9)
O(1)–C(8)–C(9)–C(14)	7.3(8)	C(9)–C(8)–N(2)–N(1)	–178.8(5)
N(2)–C(8)–C(9)–C(14)	–173.8(5)	C(7)–N(1)–N(2)–C(8)	176.4(5)
O(1)–C(8)–C(9)–C(10)	–171.8(6)	C(12)–C(13)–O(2)–C(15)	–1.5(11)
N(2)–C(8)–C(9)–C(10)	7.1(9)	C(14)–C(13)–O(2)–C(15)	178.3(6)

Table 4. Hydrogen bonds (Å and °) for 4-BRMBH crystal.

D–H···A	d(D–H)	d(H···A)	d(D···A)	<(DHA)
C(7)–H(7)···O(3)	0.93	2.50	3.304(8)	144.6
O(3)–H(3B)···O(1)$^{\#1}$	0.84(2)	1.99(3)	2.812(7)	169(8)
O(3)–H(3A)···O(1)$^{\#2}$	0.83(2)	2.08(4)	2.884(7)	161(8)
N(2)–H(2A)···O(3)	0.85(3)	2.06(3)	2.885(7)	163(7)

Symmetry transformations used to generate equivalent atoms:
$^{\#1}$ –x+1, y–1/2, –z+1/2; $^{\#2}$ –x,y–1/2, –z+1/2.

[36–39]. The dark-red spots on the d_{norm} surface arise as a result of the short interatomic contacts, *i.e.,* strong hydrogen bonds, while the other intermolecular interactions appear as light-red spots. The 2D-fingerprint plots are used to plot intercontacts with respect to d_i and d_e (Fig. 4b).

The intercontacts (quantification) were done using visualization of the Hirshfeld surfaces and 2D fingerprint plots in Fig. 4. The strong interactions in crystal intercontacts were found to be H···O (15.3%), H···H (39.5%), C···H (12.5%) and weak interactions N···H (1.9%), C···C (5.7%), N···C (5.5%), O···C (0.8%) are present. The 2D fingerprint plots of these intercontacts are shown in Fig. 5b. The major contributions are from H···H, C···H, and O···H when compared to other intercontacts. The C···C and C···H intercontacts are involved in C–H···O, N–H···O and C–O···p interactions. The dominant interactions particularly H···O, O···H are mainly responsible for maintaining charge transfer leading to nonlinearity at the micro level.

2.4. Optimization of (E)-N-(4-bromobenzylidene)-3-methoxybenzohydrazide 3

Molecular geometry, optimization of compound 4-BRMBH 3 structures, and numbering of atoms molecules are shown graphically in Fig. 1 obtained at B3LYP/6-31G* method. Table 5 shows their geometrical characteristics, including computed total energies, moments of dipoles, RMS, and maximum Cartesian force. The global minimum energies are found to be 1326.0352 a.u (36083 eV) respectively. The RMS Cartesian force value is 0.01578. It is discovered that their maximal Cartesian forces are 0.05705. A molecule's dipole moment, which represents the molecular charge distribution, is expressed as a three-dimensional vector. As a result, it may be used as a descriptor to clarify the movement of charges inside molecules. As a result of DFT/B3LYP/6-31G* calculations, the smallest dipole moment was observed for compound 3 (3.315386 Debye) Of course, the addition of other atoms has an influence on their stability. Moreover, it promotes the formation of hydrogen bonds.

2.5. Frontier orbitals and quantum chemical calculations (FMO)

In molecular systems, frontier molecular orbitals (FMOs) frequently take the lead in molecular systems. The HOMO and LUMO are employed in the chemical stability of the molecule. Electronic transitions and their energies difference Eg energy gap and chemical reactivity descriptors are given in (Table 5). The HOMO, LUMO

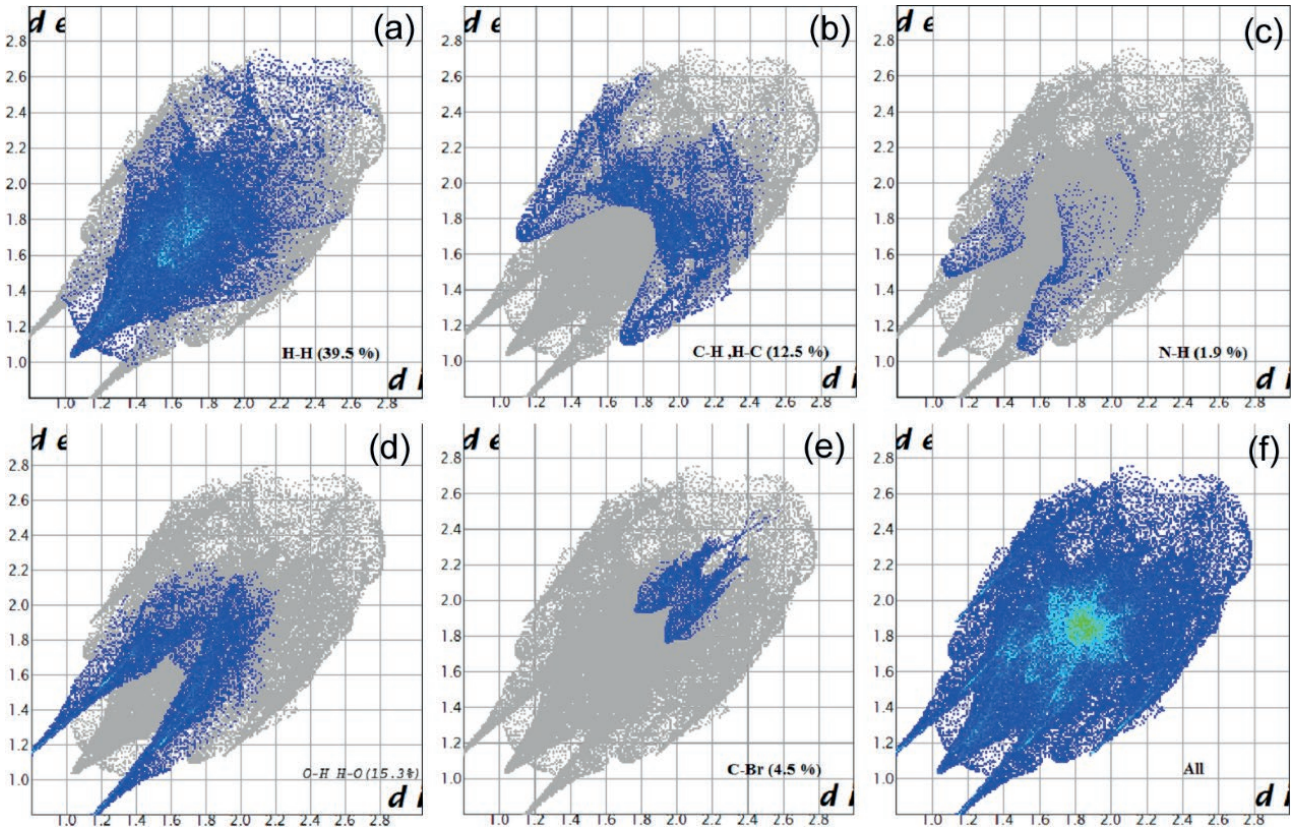

Figure 4. Fingerprint plots of 4-BRMBH crystal. All; showing reciprocal contacts and resolved into **(i)** H...H, (ii) C...H, (iii) N...H, (iv) O...H, (v) C…Br, showing the percentage contact contributing to the total Hirshfeld surface of the molecule. Black arrows are show spikes for different interactions.

energies, and band gap of present compounds are depicted in (Fig. 5).

In the present investigations, the energy gap of compound 4-BRMBH is - 4.28 eV. A small energy gap of HOMO-LUMO means more chemical activity. this decrease in gap low shows that the compound can easily flow electrons, favoring the biological activity of the compound. EHOMO illustrates the capacity for electron donation, while ELUMO illustrates the capacity for accepting electrons. The resulting tittle compound global reactivity indexes are calculated and summarized in Table 6. The electronic chemical potential of 6.12 eV. The analysis of the global electrophilicity and nucleophilicity indexes helps in describing the biological activity of the molecule, shows that compound 3 acts as a strong electrophile (ω = 1.86 eV) and a strong nucleophile (N = 3.65 eV). Analysis of the global CDFT indices confirms that 3 has a higher electrophilic and nucleophilic character which does allow it participation in polar processes. Their 3D plots are illustrated in Fig. 5. It is clear from the figure of the acridine molecule that the HOMO and LUMO orbitals are localized essentially on the acridine and substituted systems. The density of states makes it clear that the green colour denotes the negative phase and the red colour, which corresponds to the positive phase.

Using the energies of FMOs, we calculated the reactivity descriptors of (*E*)-*N*¢-(4-bromobenzylidene)-3-methoxybenzohydrazide monohydrate molecules. A = - E_{LUMO}: represent the electron affinity; I = - E_{HOMO} represent the ionization potential and l = ½ (I + A) is the electronic chemical potential. The chemical hardness (η) is found to be 2.170 eV for compound 3, respectively. Based on the value found of the electrophilicity index, we can conclude that the (*E*)-*N*¢-(4-bromobenzylidene)-3-methoxybenzohydrazide monohydrate is a good electrophile. Therefore, it is able to accept an electron doublet in order to form bonds with another reagent which is necessarily a nucleophile. Electronegativity is also determined (χ = (I + A)/2) and it is found to be χ) = 3.980 eV.

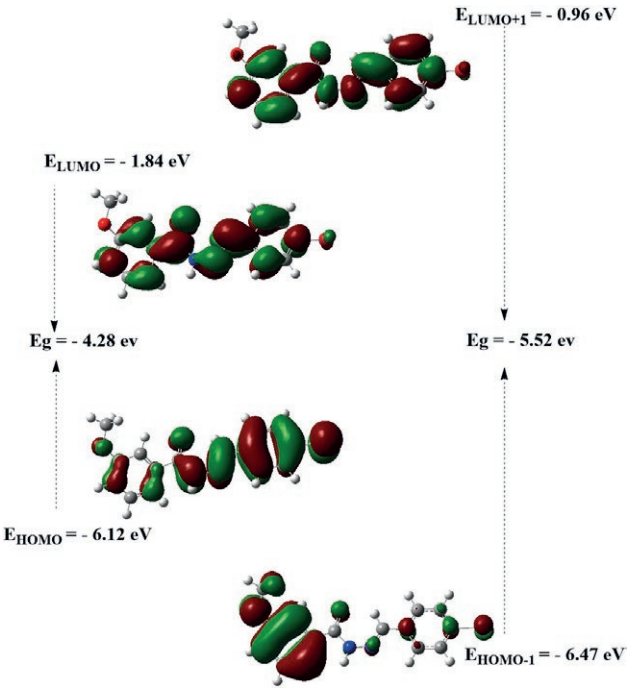

Figure 5. Energy level of EHOMO, ELUMO and Egap for the synthesized compounds **3** computed by B3LYP/6-31 G (d,p) method.

Table 6. Global Electronic Proprieties and Reactivity Indexes at 4 Compounds (in eV).

E LUMO	= - 1.84
E HOMO	= - 6.12
E HOMO -E LUMO (Eg)	= - 4.28
E LUMO +1	= - 0.96
E HOMO-1	= - 6.47
E HOMO-1 - E LUMO +1	= - 5.52
Reactivity descriptors	
Ionization potential (I)	= 6.12
Electron affinity (A)	= 1.84
Chemical hardness (η)	= 2.170
Chemical softness (x) = 1.070	
electronic chemical potential (μ)	= - 3.980
Electronegativity (χ)	= 3.980
global electrophilicity (ω)	= 3.650
Maximum charge transfer index D N Max = 1.86	

2.6. Molecular electrostatic potential surface

The molecular electrostatic potential (MEP) is an elucidation tool the complete information of molecular properties and intermolecular interactions, it allows us to electrophilic and nucleophilic sites in the molecular system reactive biological activities, these sites provide

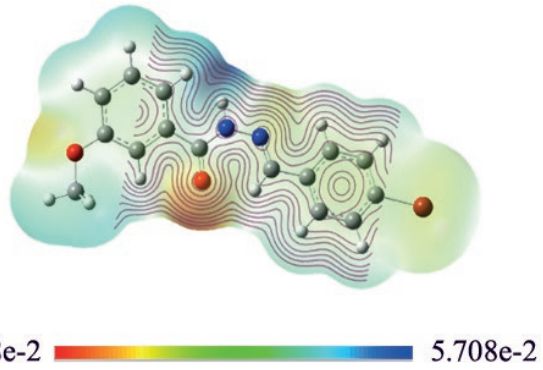

Figure 6. MEP formed by mapping of total density over electrostatic potential in gas phase for the synthesized compounds **3**

electrophilic site indicates a strong attraction, while the nucleophilic site indicates a strong repulsion and polar and nonpolar sites of the molecule in color variations as shown in a pictorial form (Fig. 6). The regions of the molecule with positive values of the electrostatic potential are indicated by blue color, the red color characterizes electrophilic reactivity (most negative). The green and gray colors correspond to an intermediate potential situated between the two extremes (red and dark blue). The yellow and light blue colors split the difference between the medium color (green) and the extremes (red/dark blue). As a result, MEP surfaces area between -7.623e-2 a.u (deepest red) to 7.623e-2 a.u (deepest blue) molecule (Fig. 5), a maximum positive region is localized on the nitrogen N and hydrogen H atoms indicating a possible site for positive potential (blue and light blue) sites are found in the benzene and pyridine rings (electrophilic reactivity). From the MEP plots, it was concluded that the oxygen of hydroxy possessed high electropositive potential (red) and the activated possessed slightly low electropositive region (blue).

(DOS) spectrum (Fig. 7) characterizes the energy levels per unit energy increment and its composition in energy. The green and red lines in these graphs, corresponding to the displaying study per orbital, describe the HOMO and LUMO energy levels, respectively. As a result, the energy level of the HOMO orbital is about - 6.162eV, and the energy level of the LUMO orbital is about -1.84 eV. The HOMO-LUMO gap energy (Eg) of compound 3 is equal to 4.28 eV. This low energy value promotes the transfer of electrons in the acridine molecule. These values are compatible with those obtained by the DOS spectrum. The state HOMO-1 form another set of degenerate orbitals - 6.47 eV and +LUMO orbital lying at -0.96 eV, located on all the atoms of the rings. Eg close to - 5.52 eV in solution involves an expected high reactivity for compound 4-BRMBH.

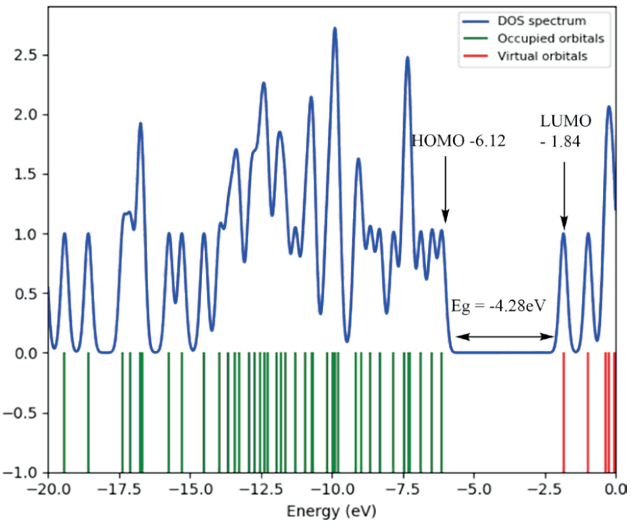

Figure 7. DOS spectrum of (E)-N¢-(4-bromobenzylidene)-3-methoxybenzohydrazide 3.

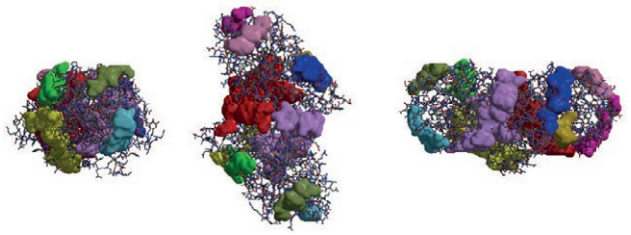

Figure 8. The docked ligand compound **3** at the same catalytic site receptor.

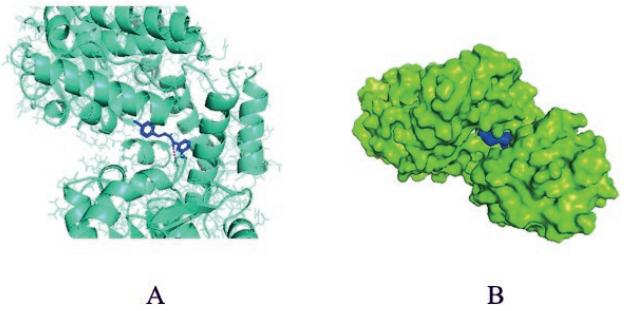

Figure 9. A) Orientation of compound 4-BRMBH in the active sites of tuberculosis proteins PDB ID: 7vjt B) The docking poses of 3 in the binding site with Surface area.

Computational results related to ^{1}H NMR spectrum of H atom camB3LYP/6-311+g(d) (ppm) Experimental (ppm) Calculated and experimental FT-IR spectra. In this work, the B3LYP/6- 311 G (d,p) theoretical model was used to obtain the ground state geometries of selected compound 3 in vacuo. Frequency calculations showed that there were no imaginary frequencies, which indicates that the stationary points correspond to the equilibrium geometries. The calculated molecular geometry was used as an input structure for further calculations IR for better understanding of electronic properties, the theoretical spectra have been calculated by TDDFT/B3LYP method.

2.7. Molecular docking

Docking studies were carried out to find the potential binding affinity and the interaction between the compounds for receptor protein as shown in Figs. 8-10. Compound 4-BRMBH has van der Waals interactions with surrounding hydrophobic residues Try1637, Phe1670, Met1669, Asp1666, Thr1589, Lys1588, Ser1636 and Phe1585. In compound Asn1640 is bridged through H_2O forming hydrogen bonds through hydrazide group. The study also revealed that the benzohydrazide scaffolds are the key residues at the active site of prostate cancer, anti-tuberculosis etc. Moreover, compounds have minimum binding energy, which could be considered as a good inhibitor. The synthesized compounds were found to display good binding affinity to the receptor with minimum binding energy equal to –9.70 kcal/mol. From docking studies, we found that the compound showed highest glide score –9.27 kcal/mol and glide energy of –42.126 kcal/mol respective and their docking scores are shown in Table 7. These *in silico* results

Table 7. Molecular docking results showing CDock score and types of interactions.

Compound id	CDocker Energy	Type and number of interactions	Residues involved
4-BRMBH	–27.28	van der Waals interaction-1	Between –OCH_3 of methoxy benzo hydrazide and of amino acid residue: LYS: 165
		van der Waals interaction-1	Between –C=O of methoxy benzo hydrazide and of amino acid residue: ILE: 194
Iisoniazid (Standard)	–22.1896	Electrostatic interaction-2	Between –C=O of benzo hydrazide and of amino acid residue LYS A: 165
		van der Waals interaction-1	Between hydrogen of benzohdrazide and LYS A: 165 of amino acid residue. Between hydrogen of benzohydrazide and of amino acid residue ASP: 148

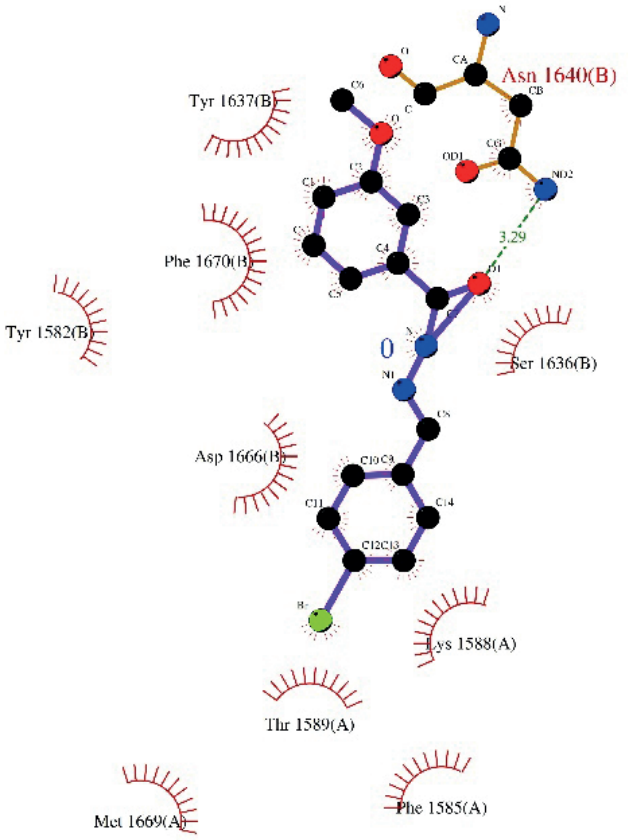

Figure 10. LigPlot+ Interaction of compound 4-BRMBH with 7vjt.

revealed that the synthesized benzohydrazide compounds may be an effective drug candidate for antituberculosis.

The 3D crystal structure of the enzyme reported in this work was downloaded from the Protein Data Bank (PDB id: 7vjt) and was processed by the addition of hydrogen, assigning the bond order, identifying overlaps, creating zero order bonds to metals and creating disulfide bonds. The 2D structures of the synthesized ligands were drawn from Chem Draw and saved as mol format and was examined so as to generate the best pose by analyzing the binding interactions. After the generation of the grid, the ligands synthesized were docked to identify the interaction with the active site of the protein. The scoring functions and hydrogen bonds formed with the surrounding amino acids were used to predict their binding modes, their binding affinities and orientation of these compounds at the active site of *Mycobacterium tuberculosis* InhA protein.

In order to find suitable inhibitor for *M. tuberculosis* docking studies was carried out for InhA protein. The enoyl-ACP reductase from *M. tuberculosis*, known as InhA, was a member of an unusual FAS-II system that prefers longer chain fatty acyl substrates for the purpose of synthesizing mycolic acids, a major component of mycobacterial cell walls. Mycolic acids, which were essential building blocks of the waxy cell wall of mycobacteria. Inhibition of InhA blocks mycolic acid biosynthesis, thereby impairing the integrity of the cell wall and eventually leading to cell death [40 - 42]. New compounds that directly target InhA and dodge the activation step are promising candidates for combating multidrug-resistant strains of *M. tuberculosis*. There was a structural similarity between the synthesized compound and isoniazid, one of the standard antimycobacterial references. Therefore, the docking results of 4-BRMBH were compared with that of isoniazid and were tabulated in Table 7. It was observed that the CDocker score of 4-BRMBH was comparable with that of standard isoniazid. Therefore compound 4-BRMBH may be suitable to overcome the drug resistance of *M. tuberculosis*. The protein–ligand interaction study was accomplished using LigPlot. the identification of such residues leads to support the observed activity *M. tuberculosis* exhibited by the studied compounds.

2.8. ADMET analysis

In-silico prediction of pharmacokinetics and drug-likeness profiles. *Clinical trials of* newly investigated drugs are known to be read are the absorption, distribution, metabolism, excretion, and toxicity (ADMET) belongings of the compound (Table 8). The drug-likeness of the compound is accessed based on the Lipinski's rule of five (RO5) and the result shows no violation of the rule. Many parameters are studied using virtual screening methods, such as human intestinal absorption HIA, partition coefficient (log p), drug solubility (S), topological polar surface area (TPSA), cell permeability, and drug-likeness score. An available oral drug is chosen in accordance with Lipinski's rule of + ve if the molecular weight < 500, the number of hydrogen bond donors < 5, the number of hydrogen bond acceptors < 10, and Log P is <5.41 The number of rotatable bonds is used to reflect molecular flexibility, which is important for oral bioavailability. Lipinski's rule RO5 of result 0 violation showed that compound 4, possess good molecular weight (g/mol), two Hydrogen Bond Accepted and Hydrogen Bond Donor values two log P 2.45 which are significantly justified if their drug-likeness behavior were justifiable with the standard values. The RO5 deviation (Mol. Wt≥500 g/mol; HBD≥ 5; HBA > 10; and logP≥ 5). drug-likeness score is an amalgam of complex balance of several molecular properties and structure features that

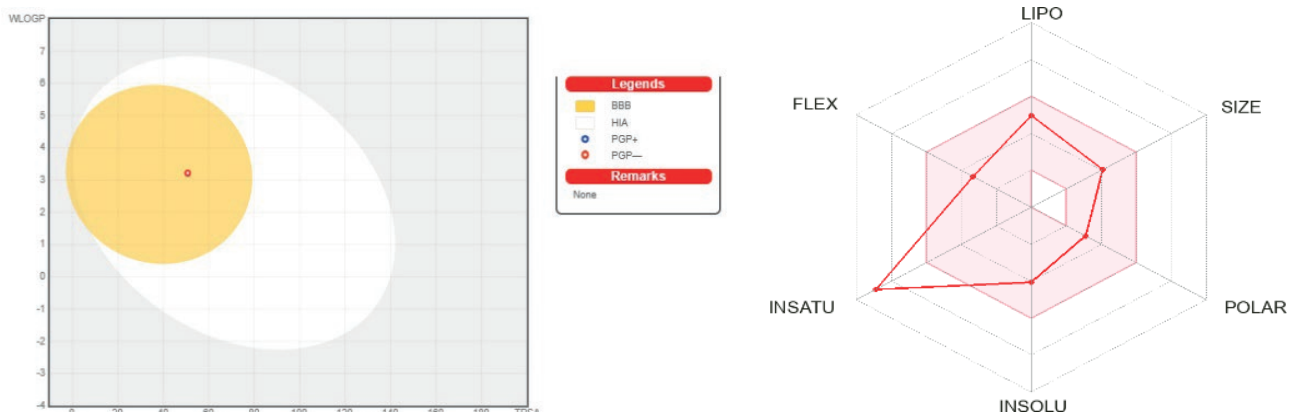

Figure 11. BOILED-Egg models and Swiss ADME bioavailability radar reports of 4-BRMBH.

determine the behaviour of molecules drug. 0.55 good drug score values, which depicted their wonderful drug-like behaviour to be suitable drug candidates against cancer protein. The results got from the Swiss ADME and Molinspiration search engine are listed in Table 8.

The same observed in the BOILED-egg diagram (Fig. 11) analysis shows that the compound is strong within the permissible range of standard drugs, where the dot in the yellow zone demonstrates blue dot indicates cannot be affected by the P-glycoprotein of the CNS system by P-glycoprotein, point locate in Boiled Eggs yolk is a molecule passively permeate through the blood–brain barrier (BBB) the red color region demonstrates the ability to stay in the brain. In the current study, the synthesized ligand and its complexes were initiated to be in a good pact with the criteria and can be said to possess good bioavailability the result proves that the compound is safe and unable to cause allergies on the skin. The drug scores of compounds, are remark clever and could be mentioned as moderate drug scores [43].

2.9. Target prediction

Nowadays, the probable targets of small molecules can be provided by established bio-/chemo-informatics approaches. Ligand-based target prediction has shown high-quality performance and the ability to quickly predict correct protein targets of compounds in drug discovery context. Predictions made using the Swiss Target web tool aim to predict the most probable protein targets of small molecules. The current analysis was restricted to the top 15 Homo sapiens targets. Molecule 3 was estimated to have a 27.7 % probability of binding enzyme receptors.

3. EXPERIMENTAL

3.1. Materials and methods

The reagents, solvents were obtained from commercial sources like Sigma-Aldrich, Spectrochem, etc. and used without further purification. The reactions were monitored by Merck silica gel 60 thin layer chromatography (TLC) and visualized in UV light chamber.

3.2. Characterization techniques

A Bruker AXS (Kappa Apex II) X-ray diffraction meter was used for single crystal XRD studies with graphite-monochromated MoKa radiation (l = 0.71073Å) at room temperature. The data collection, data reduction, and absorption correction were performed by

Table 8. Physicochemical descriptors and ADME parameters[a].

M.W g/mol	RB	H-A	H-D	TPSA	MR	*W log P (lipophilicity)*	ESOL log S	BBB Permeant	log Kp cms^{-1}	Lipinski Violations	PAINS alerts	GI absorption	Synthetic Accessibility
255.27	1	4	3	73.58 Å^2	75.09	2.73	-4.30	Yes	-5.15	0	0	High	1.74

[a]R bond =Rotatable bond, H-A = Hydrogen bond acceptor, H-D =hydrogen bond donor, TPSA = topological polar surface area, BBB = blood brain-barrier, log P = lipophilicity, log S = water solubility, log Kp = permeability coefficient, PAINS = pan-assay interference structure.

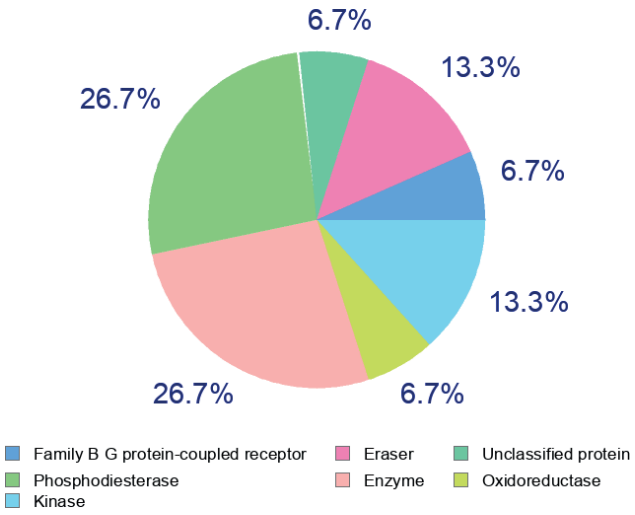

Figure 12. Swiss Ligand-based target prediction of 4-BRMBH.

APEX2. The structure was solved by the direct method procedure and the non-hydrogen atoms were subjected to anisotropic refinement by full-matrix least squares on F^2 using SHELXL-2016 [4]. The ^{1}H and ^{13}C NMR spectra were recorded in Bruker AVANCE II at 400 MHz respectively using DMSO-d_6 solvent at room temperature. The morphology of the crystals was examined with a JEOL JSM-5610 scanning electron microscope (SEM) is outfitted with BE detector [12]. Thermo gravimetric and differential thermal analysis (TG-DTA) was carried out using a NETZSCH STA 449 F3 thermal analyzer in the nitrogen atmosphere.

3.3. Computational studies

The theoretical calculations were carried out using the Gaussian 09W program package [13]. The geometry using density functional group theory (DFT) B3LYP method with LANL2MB as the basis set. Using the GaussView 09 molecular visualization program [14,15], the optimized structure of the molecules have been visualized. Polarizability and first-order molecular hyperpolarizability were premeditated by using finite field method as default with DFT method 6-311G (d, p) as basis set [16–19]. The density of states (DOS) plots was obtained by using Gauss-Sum software. Global electronic proprieties, HOMO and LUMO, energy gap (DE), electronegativity (c) and reactivity indexes, including electronic chemical potential (μ), chemical hardness (η), softness (s), ionization potential (I), electron charge transfer (DN) global electrophilicity (ω), and global nucleophilicity N were computed by the following expressions: μ = (EHOMO + ELUMO)/2 and η = (ELUMO − EHOMO), ω = μ2/2η, and N = EH − EH(TCE). The Parr functions were used to calculate the local reactivity indexes, namely, local electrophilic (Pk+), and nucleophilic (Pk–), via the analysis of the Mulliken atomic spin density (ASD) all these global molecular reactivity descriptors are estimated from the optimized structures.

Hirshfeld surfaces and fingerprint plots were generated from the CIF files of the desired compounds using the Crystal Explorer (Version 3.1). Intermolecular distance information on the surface can be shown in a two-dimensional histogram of d_e and d_i, which is a unique identifier for molecules in a crystal structure, and is known as a fingerprint plot [20, 21].

3.4. In-silico *molecular docking*

Molecular docking studies were carried out by using Schrodinger software [22]. The protein structure of the androgen receptor (PDB:7vjt) were obtained from RCSB Protein Data Bank with the resolution of 1.70 Å and prepared using Protein Preparation Wizard in Maestro 11.2. OPLS-2005 was used for the optimization and minimization until root mean square deviation reached 0.3 Å [23]. Further grid was formed in the protein using Receptor grid generation. The ligands 4-BRMBH were prepared using ligand preparation wizard and optimized the structures. The docking was carried out using the ligand docking module with an extra precession method using GLIDE XP [24–26].

3.5. General procedure for synthesis of (E)-N'-(4-bromobenzylidene)-3-methoxybenzohydrazide

The hydrazone derivative used in the present work (Scheme 1). The 4-BRMBH single crystals were grown at room temperature. A mixture of 3-methoxybenzohydrazide (2.20g, 2 mmol), and 4-bromobenzaldehyde (3.66g, 2 mmol), and 1 ml of aceticacid in methanol (50 ml) were developed and the solution was blended to create a homogenous solution at room temperature for 3 h. TLC verified the completion of the reaction. The solution was filtered, slightly warmed and allowed to evaporate very slowly. The crystallization took place within a period of 4–5 days and the grown yellow color crystals were harvested. Under reduced pressure, excess solvent was evaporated and the material (I) remaining was under reduced pressure, excess solvent was evaporated and the left material (I) recrystallized from methanol.

3.6. X-ray crystallography

Data collection of $C_{15}H_{15}BrN_2O_3$ was performed using STOE IPDS 2 diffractometer equipped graphite

monochromatic MoKa radiation 296 K [27]. The structure solution was solved by means of SHELXT [28] and refinement were carried out on F^2 by full matrix least square technique. For obtaining the visualization, Mercury Window [29] was used. The other two programs employed in preparation for publication are WinGX [30] and pubCIF [31]. A riding model was used for refinement of all hydrogen atoms C–H and NH atoms. Also PLATON [32] software was used to investigate the hydrogen bond in the crystal. The experimental details for $C_{15}H_{15}BrN_2O_3$ were summarized in Table 1.

3.7. DFT calculations

The GaussView program was applied to model the initial structures of (*E*)-*N*¢-(4-bromobenzylidene)-3-methoxybenzohydrazide monohydrate **3**. Then, their molecular optimizations of geometries were carried out in the gas phase with the density functional theory (DFT) with the Gaussian 09 software package [23]. All the quantum-chemical calculations have been performed using the hybrid B3LYP Becke's Three Parameter Hybrid Functional using the Lee Yang-Parr correlation functional at 6-31G (d, p) basis set [24, 25]. Furthermore, several electronic properties for instance the frontier molecular orbitals, gap energies, and reactivity descriptors.

The density of states (DOS) plots was found by using Gauss-Sum software programm. Global electronic proprieties, HOMO and LUMO, energy gap (DE), electronegativity (c) and reactivity indexes, including electronic chemical potential (μ), chemical hardness (η), softness (s), ionization potential (I), electron charge transfer (DN) global electrophilicity (ω), and global nucleophilicity N were computed by the following expressions: μ = (EHOMO + ELUMO)/2 and η = (ELUMO − EHOMO), ω = μ2/2η, and N = EH − EH(TCE). The Parr functions were used to calculate the local reactivity indexes, namely, local electrophilic (Pk+), and nucleophilic (Pk–), via the analysis of the Mulliken atomic spin density (ASD) all these optimized structures are utilized to estimate these global molecular reactivity characteristics.

3.8. ADME/Tox profile

ADME/Tox is used to predict important capacity to properties evaluate necessary Lipinski's rule. The rule is beneficial for developing a prospective therapeutic molecule and designing drugs. SWISS ADME and molinsperation predictor web server tool to describe, molecular weight, Rotatable bonds, hydrogen bond acceptor, hydrogen bond donor (HBDs), absorption, distribution, molar refractivity, topological polar surface area (TPSA), water solubility (log S), lipophilicity, blood brain-barrier, skin permeability (log Kp), synthetic accessibility score (SA), percentage absorption, pharmacokinetics, drug- lead likeness. The use of these representations has specifically been contributive to drug optimization and avoiding late-stage failures.

CONCLUSION

In this present work, we have synthesized 4-BRMBH crystal and successfully grown from the solvent's methanol by slow evaporation technique. The structure of small molecules was determined by NMR and single crystal XRD analysis. The crystal structure is elucidated by with a $P2_12_12_1$ space group. Theoretical calculations by DFT clearly support the experimental observations. The intermolecular interactions in the crystal structures were quantified using the Hirshfeld surface analysis, and the molecular docking studies, results showed that the compounds had very good binding affinity to receptor protein (7VJT) which can be a potent molecule for antituberculosis. ADMET prediction indicated that drug-likeness outlines of the compound. As a result, it is possible to say that compound 3 as suitable applicant for the development of the new *M. tuberculosis* agent. The above remarkable considerations and pharmaceutical applications prompted us to give vital information for further development.

AUTHORS CONTRIBUTIONS

All authors (K Ananthi, H Anandalakshmi, A Nepolraj and S Akshaya) have contributed equally to writing and reviewing the manuscript.

FUNDING

The authors thank RUSA 2.0 for providing funds to carry out the research successfully.

REFERENCES

[1] N.G. Kandile, M.I. Mohamed, H.M. Ismaeel, Synthesis of new Schiff bases bearing 1,2,4-triazole, thiazolidine and chloroazetidine moieties and their pharmacological evaluation, *J. Enzyme Inhib. Med. Chem.,* **2017**, 32, 119–129. https://doi.org/10.1080/14756366.2016.1238365

[2] U. Casellato, P.A. Vigato, M. Vidali, Transition metal complexes with binucleating ligands, *Coord. Chem. Rev.,* **1977** 23, 31–117. https://doi.org/10.1016/S0010-8545(00)80330-6

[3] K. Dey, A.K. Biswas, A. Roy, Metallic complexes as ligands: Part II-Nickcl(II) complex of the Schiff base derived from 3-formylsalicylic acid and ethylenediamine as ligand for Ti, Zr, Sn, P and B, *Indian J. Chem.,* **1981**, 20A, 848–851.

[4] L. Pogany, J. Moncol, M. Gal, I. Salitros, R. Boca, Four cobalt (III) Schiff base complexes – Structural, spectroscopic and electrochemical studies, *Inorg. Chim. Acta.,* **2017** 462, 23–29. https://doi.org/10.1016/j.ica.2017.03.001

[5] C. M. da Silva, D. L. da Silva, L. V. Modolo, R. B. Alves, M. A. Deresede, C. V. Martin, A. Defatima, Schiff bases: A short review of their antimicrobial activities, *J. Adv. Res.,* **2011**, 2, 1–8. https://doi.org/10.1016/j.jare.2010.05.004

[6] M. Andruh, Compartmental Schiff-base ligands – a rich library of tectons in designing magnetic and luminescent materials, *Chem. Commun.,* **2011**, 47, 3025–3042. https://doi.org/10.1039/C0CC04506C

[7] M. Sarigul, A. Sari, M. Kose, V. McKee, M. Elmastas, I. Demirtas, M. Kurtoglu, New bio-active azo-azomethine based Cu (II) complexes, *Inorg. Chim. Acta.,* **2016,** 444, 166– 175. https://doi.org/10.1016/j.ica.2016.01.042

[8] H. Keypour, M. Shayesteh, M. Rezaeivala, F. Chalabian, Y. Elerman, O. Buyukgungor, Synthesis, spectral characterization, structural investigation and antimicrobial studies of mononuclear Cu(II), Ni(II), Co(II), Zn(II) and Cd(II) complexes of a new potentially hexadentate N_2O_4 Schiff base ligand derived from salicylaldehyde, *J. Mol. Struct.,* **2013** 1032, 62–68. https://doi.org/10.1016/j.molstruc.2012.07.056

[9] D. Chen, A.E. Martell, Dioxygen affinities of synthetic cobalt Schiff base complexes, *Inorg. Chem.,* **1987**, 26, 1026–1030. https://doi.org/10.1021/ic00254a013

[10] D. Chen, A.E. Martell, Y. Sun, New synthetic cobalt Schiff base complexes as oxygen carriers, *Inorg. Chem.,* **1989**, 2, 2647–2652. https://doi.org/10.1021/ic00312a029

[11] K. Durka, A.A. Hoser, R. Kaminski, S. Lulinski, J. Serwatowski, W. Kozminski, K. Wozniak, Polymorphism of a model arylboronicazaester: Combined experimental and computational studies, *Cryst. Growth. Des.,* **2011**, 11, 1835–1845. https://doi.org/10.1021/cg200032e

[12] M. Behzad, L. SeifikarGhomi, M. Damercheli, B. Mehravi, M. ShafieeArdestani, H. SamariJahromi, Z. Abbasi, Crystal structures and *in vitro* anticancer studies on new unsymmetrical copper(II) Schiff base complexes derived from meso-1,2-diphenyl-1,2- ethylenediamine: a comparison with related symmetrical ones, *J. Coord. Chem.,* **2016**, 69, 2469–2481. https://doi.org/10.1080/00958972.2016.1198786

[13] Y. L. Zhang, W. J. Ruan, X. J. Zhao, H. G. Wang, Z. A. Zhu, Synthesis and characterization of axial coordination cobalt (III) complexes containing chiral Salen ligands, *Polyhedron,* **2003,** 22, 1535–1545. https://doi.org/10.1016/S0277-5387(03)00261-4

[14] Z. Abbasi, M. Behzad, A. Ghaffari, H. AmiriRudbari, G. Bruno,Mononuclear and dinuclearsalen type copper(II) Schiff base complexes: Synthesis, characterization, crystal structures and catalytic epoxidation of cyclooctene, *Inorg. Chim. Acta.,* **2014**, 414, 78–84. https://doi.org/10.1016/j.ica.2014.01.047

[15] M. R.V. Jørgensen, I. Skovsen, H. F. Clausen, J. L. Mi, M. Christensen, E. Nishibori, M. A. Spackman, B. B. Iversen, *Inorg. Chem.,* **2012**, 51, 1916–1924. https://doi.org/10.1021/ic202231k

[16] Y. H. Luo, B. W. Sun, An investigation into the substituent effect of halogen atoms on the crystal structures of indole-3-carboxylic acid (ICA), *CrystEngComm.,* **2013**, 15, 7490–7497. https://doi.org/10.1039/C3CE40952J

[17] A. Ghaffari, M. Behzad, M. Pooyan, H. AmiriRudbari, G. Bruno, Crystal structures and catalytic performance of three new methoxy substituted salen type nickel (II) Schiff base complexes derived from *meso*-1,2-diphenyl-1,2-ethylenediamine, *J. Mol. Struct.,* **2014**, 1063, 1–7. https://doi.org/10.1016/j.molstruc.2014.01.052

[18] H. C. Wang, X. Q. Yan, T. L. Yan, H. X. Li, Z. C. Wang, Design, synthesis and biological evaluation of benzohydrazide derivatives containing dihydropyrazoles as potential EGFR kinase inhibitors, *Molecules.* **2016**, 21, 1012. https://doi.org/10.3390/molecules21081012

[19] B. Rigo, D. Couturier, Studies on pyrrolidinones. Synthesis of 5-(5-oxo-2-pyrrolidinyl)-1,3,5-oxadiazole-2-thione derivatives, *Heterocycl. Chem.,* **1985**, 22, 287–288. https://doi.org/10.1002/jhet.5570220209

[20] M. Somashekhar, Synthesis and antimicrobial activity of 4-(morpholin-4-yl) benzohydrazide derivatives. *World J. Pharm. Pharm. Sci.,* **2013**, 2, 2011–2020.

[21] P. Nun, C. Martin, J. Martinez, F. Lamaty, Solvent-free synthesis of hydrazones and their subsequent N-alkylation in a Ball-mill, *Tetrahedron*, **2011**, 67, 8187–8194. https://doi.org/10.1016/j.tet.2011.07.056

[22] P. Melnyk, V. Leroux, C. Sergheraert, P. Grellier, *Bioorg. Med. Chem. Lett.,* **2006**, 16, 31–35. https://doi.org/10.1016/j.bmcl.2005.09.058

[23] I. Afreen, M. Sonam, S. R. Maitreyi, A. Fernando, A. Amir, Synthesis and biological evaluation of 4-(2-(dimethylamino)ethoxy) benzohydrazide derivatives as inhibitors of *Entamoebahistolyica*, *Eur. J. Med. Chem.,* **2016**, 124, 445–455. https://doi.org/10.1016/j.ejmech.2016.08.022

[24] K. K. Bedia, O. Elcin, U. Seda, K. Fatma, S. Nathaly, Synthesis and characterization of novel hydrazide-hydrazones and the study of their structure-antituberculosis activity, *Eur. J. Med. Chem.,* **2006**, 41, 1253–1261. https://doi.org/10.1016/j.ejmech.2006.06.009

[25] H. Lgaz, I.-M. Chung, M. R. Albayati, A. Chaouiki, R. Salghi, S. K. Mohamed, Improved corrosion resistance of mild steel in acidic solution by hydrazone derivatives: An experimental and computational study, *Arab. J. Chem.,* **2018**, 2934–2954. https://doi.org/10.1016/j.arabjc.2018.08.004

[26] H. Lgaz, A. Chaouiki, M. R. Albayati, R. Salghi, Y. El Aoufir, I. H. Ali, M. I. Khan, S. K. Mohamed, I.-M. Chung, Synthesis and evaluation of some new hydrazones as corrosion inhibitors for mild steel in acidic media, *Res. Chem. Intermed.,* **2019**, 45, 2269–2286. https://doi.org/10.1007/s11164-018-03730-y

[27] Stoe and Cie, X-AREA (Version 1.18.) and X-RED32 (Version 1.04.), Stoe and Cie, Germany, Darmstadt, **2002**.

[28] G.M. Sheldrick, SHELXT: Integrating space group determination and structure solution, *ActaCrystallogr.* **2015**, A 71, 3–8. https://doi.org/10.1107/S2053273314026370

[29] C. F. Macrae, I. J. Bruno, J. A. Chisholm, P. R. Edgington, P. McCabe, E. Pidcock, L. Rodriguez-Monge, R. Taylor, J. van de Streek, P.A. Wood, Mercury CSD 2.0–new features for the visualization and investigation of crystal structures, *J. Appl. Crystallogr.* **2008,** 41, 466–470. https://doi.org/10.1107/S0021889807067908

[30] L. J. Farrugia, WinGX suite for small-molecule single-crystal crystallography, *J. Appl. Crystallogr*. **1999**, 32, 837–838. https://doi.org/10.1107/S0021889899006020

[31] S. P. Westrip, publCIF: software for editing, validating and formatting crystallographic information files, *J. Appl. Crystallogr,* **2010**, 43, 920–925. https://doi.org/10.1107/S0021889810022120

[32] A. Spek, Single-crystal structure validation with the program PLATON, *J. Appl. Crystallogr.* **2003**, 36, 7–13. https://doi.org/10.1107/S0021889802022112

[33] J. J. McKinnon, M. A. Spackman, A. S. Mitchell, Novel tools for visualizing and exploring intermolecular interactions in molecular crystals, *J. ActaCrystallogr.* **2004**, B 60, 627–668. https://doi.org/10.1107/S0108768104020300

[34] M. A. Spackman, D. Jayatilaka, Hirshfeld surface analysis, *CrystEngComm.,* **2009**, 11, 19–32. https://doi.org/10.1039/B818330A

[35] M. Venkateshan, R. Vishnu Priya, M. Muthu, J. Suresh, R. Ranjith Kumar, Crystal structure, Hirshfeld surface analysis, DFT calculations and molecular docking studies on pyridine derivatives as potential inhibitors of NAMPT, *Chem. Data Collect.,* **2019**, 23, 100262. https://doi.org/10.1016/j.cdc.2019.100262

[36] C. Lee, W. Yang, R.G. Parr, *Phys. Rev.,* **1988**, B 37, 785–789. https://doi.org/10.1103/PhysRevB.37.785

[37] A.M. K€oster, M. Leboeuf, D.R. Salahub, in: S.M. Jane, S. Kalidas (Eds.), Molecular electrostatic potentials from density functional theory, *Theor. Comput. Chem.,* **1996**, 105–142. https://doi.org/10.1016/S1380-7323(96)80042-2

[38] M. A. Spackman, J. J. McKinnon, Fingerprinting intermolecular interactions in molecular crystals, *CrystEngComm*., **2002,** 4, 378–392. https://doi.org/10.1039/B203191B

[39] S. Madan Kumar, B.C. Manjunath, G.S. Lingaraju, M.M.M. Abdoh, M.P. Sadashiva, N.K. Lokanath, A Hirshfeld surface analysis and crystal structure of 2¢-[1-(2-fluorophenyl)-1H-tetrazol-5-yl]-4-methoxybiphenyl-2-carbaldehyde, *Cryst. Struct. Theor. Appl.,* **2013**, 3, 124–131. DOI: 10.4236/csta.2013.23017

[40] A. Denise Rozwarski, C. Vilcheze, M. Sugantino, R. Bittman, J.C. Sacchettini, *J. Biol. Chem.,* **1999**, 274, 15582–15589. https://doi.org/10.1074/jbc.274.22.15582

[41] R. Maheswari, J. Manjula, Vibrational spectroscopic analysis and molecular docking studies of (E)-4-methoxy-N-(4-methylbenzylidene) benzohydrazide by DFT, *J. Mol. Struct.,* **2016**, 1115, 144–155. https://doi.org/10.1016/j.molstruc.2016.02.066

[42] M.I. Okeke, C.U. Iroegbu, E.N. Eze, A.S. Okoli, C.O. Esimone, Evaluation of extracts of the roots of *Landolphiaowerrience* for antibacterial activity, *J. Ethnopharmacol.,* **2001**, 78, 119–127. https://doi.org/10.1016/S0378-8741(01)00307-5

[43] A. Nepolraj, V. I. Shupeniuk, M, Sathiyaseelan N. Prakash. Synthesis of new 3-(hydroxymethyl)-2-phenyl-2, 3 dihydroquinolinone and in-silico evaluation of COVID-19 main protease inhibitor. *Vietnam J Chemistry.,* **2021,** 59, 511-521 https://doi.org/10.1002/vjch.202000221